

# DNA nano-mechanics: how proteins deform the double helix

Nils B. Becker\*

Laboratoire de Physique de l'École Normale Supérieure,  
Université de Lyon, France

Ralf Everaers

Laboratoire de Physique de l'École Normale Supérieure,  
Université de Lyon, France

October 29, 2018

## Abstract

It is a standard exercise in mechanical engineering to infer the external forces and torques on a body from a given static shape and known elastic properties. Here we apply this kind of analysis to distorted double-helical DNA in complexes with proteins: We extract the local mean forces and torques acting on each base-pair of bound DNA from high-resolution complex structures. Our analysis relies on known elastic potentials and a careful choice of coordinates for the well-established rigid base-pair model of DNA. The results are robust with respect to parameter and conformation uncertainty. They reveal the complex nano-mechanical patterns of interaction between proteins and DNA. Being non-trivially and non-locally related to observed DNA conformations, base-pair forces and torques provide a new view on DNA-protein binding that complements structural analysis.

## Introduction

A large class of DNA-binding proteins induce deformations of the DNA double helix which are essential in biochemical processes such as transcription regulation, DNA packing and replication [1]. Insight into the mechanism of binding largely depends on high-resolution structures of DNA-protein complexes. A first step in their analysis consists of a description of DNA conformation in the complex, often in terms of a suitably reduced set of degrees of freedom such as the rigid base-pair parameters, e.g. [2]. As a second step, sites of local DNA deformation can be identified by comparison with ensembles of fluctuating DNA conformations. This allows to quantify deformation strength in terms of a free energy. Here we take the analysis a step further by extracting the points of attack, magnitudes and directions of forces acting between protein and DNA in the complex.

The basic idea of inferring the force on an elastic body from its deformation is as commonplace as stepping on a scale to measure one's weight. We propose to apply the same idea to DNA-protein complexes, using DNA as a nanoscale force probe calibrated by a known elastic potential. That is, starting

---

\*Corresponding author. Address: Labo de Physique de l'ENS, 46 allée de l'Italie, 69007 Lyon, France

from the coarse-grained mean conformation of a piece of bound DNA as extracted from a high-resolution structural model, we infer the corresponding coarse-grained static mean forces required for that conformation. To implement this idea, we use the rigid base-pair level of coarse-graining. Correspondingly, our analysis results in a DNA base-pair step elastic energy profile, complemented by the set of mean forces and torques by which the protein acts on each DNA base-pair.

This article focuses on the theoretical basis, implementation, range of applicability and validation of DNA nano-mechanics analysis. We begin by discussing the statistical mechanics of the mechanical equilibrium in DNA-protein complexes in section Background. We also motivate our choice of the rigid base-pair level of coarse-graining which, unlike standard molecular mechanics with atomistic force fields, allows reliable extraction of mean forces within the experimentally available resolution. Our matrix formalism for force and torque calculations is described in section DNA nano-mechanics, and implementation and parameter choice details are given in Methods. In the Results section, we present exemplary force and torque calculations for several high-resolution NMR and x-ray complex structures. These examples show the robustness of the analysis with respect to experimental and parameter uncertainties, and demonstrate the key features of base-pair forces and torques described in the Discussion section: Base-pair forces and DNA deformation are nontrivially and non-locally related, and they allow to discriminate force-transmitting and non-transmitting protein-DNA contacts. Based on these features, DNA nano-mechanics analysis has a number of promising applications, such as validation and design of coarse-grained molecular models for multi-scale simulations, and identification of target sites for structure-changing mutations in protein-DNA complexes. These are expanded upon in the

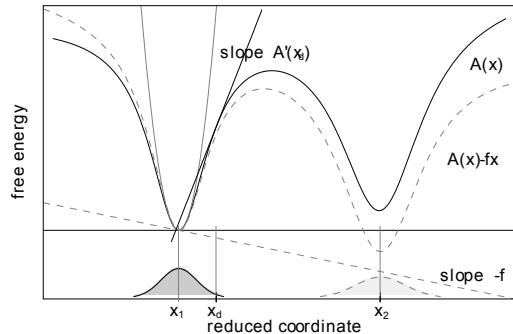


Figure 1: Constraint force  $f_d$  and externally applied force  $f$  in a stereotyped double-well free energy landscape, and thermal distribution (solid lines). Under an external force  $f$ , the landscape is tilted (dashed lines).

Conclusion section.

## Background

The statistical mechanics of DNA can be described on multiple levels of coarse-graining, depending on the required amount of detail. For a chosen set of reduced coordinates  $\{x\}$ , the corresponding free energy  $A(x)$  is a potential of mean force, i.e. constraining the system to a conformation  $x_d$  requires the mean force  $f_d = A'(x_d)$ . This holds regardless whether or not  $A$  is approximately quadratic; for instance,  $A$  could have a shape as in Fig. 1.

From high-resolution structures of protein-DNA complexes one obtains the mean conformation  $x_d$  within some uncertainty  $\delta_d$ , and the size  $B^{1/2} = \langle (x - x_d)^2 \rangle^{1/2}$  of thermal fluctuations around it. If the force is approximately linear over the range  $B^{1/2}$ , i.e. if

$$A''' < 2A'/B, \quad (1)$$

then the mean force by which the environment acts upon DNA to produce the observed conformation is given as  $f_d = A'(x_d) \pm A''(x_d)\delta_d$ . This simple scheme fails for atomistic force fields since they are strongly nonlinear on the

$B^{1/2} \gtrsim 5 \text{ \AA}$ , violating Ineq. 1. Mean atomistic forces would have to be extracted from a full MD simulation with adequately constrained average (not instantaneous) positions. In contrast, mean forces acting on groups of atoms may be meaningfully extracted from coarse-grained descriptions of a single structure, when the smoother coarse-grained free energy is compatible with Ineq. 1.

Here we consider the rigid base-pair [3] model of DNA as a good compromise between resolution and reliability. The corresponding sequence-dependent free energies have been parametrized from microscopic data [4, 5] with considerable effort. They have been successfully used in describing indirect readout [6, 7, 8, 9] and match well with known,  $\mu\text{m}$  scale DNA elastic properties [10]. The free energy functions, and therefore the extracted forces, are reliable within some sufficiently sampled region around the ideal B-DNA ground state which excludes only the most extreme deformations, see Discussion. Notably, the sampled free energy within this region is well approximated by a quadratic function [5, 4], leading to linear elastic forces and validity of Ineq. 1. While extensions of the free energy function into the anharmonic region and inclusion of trinucleotide coupling could further improve on the range of validity and accuracy base-pair forces, the present parametrization leads to consistent results, as shown below. Note that by choosing the rigid base-pair level of coarse-graining, all information on force pairs that cancel on smaller scales, e.g. separation of bases, is disregarded. The resulting description retains those forces that are relevant for large scale DNA deformations.

## DNA nano-mechanics

In the rigid base-pair model of DNA [3], base-pairs are represented by as rigid bodies with-

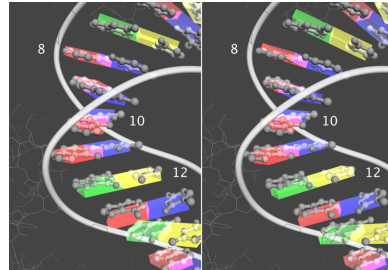


Figure 2: Rigid base-pair model. Atomic coordinates are reduced to the base-pair center position and orientation degrees of freedom, represented as bricks. Conformations of the *Ipp*-I complex before (left) and after (right) pre-relaxation within a range of  $r_m = 0.3\text{\AA}$ , see Methods.

out internal structure, see Fig. 2. From the atomic coordinates of a base-pair  $k$ , a reference frame  $\mathbf{g}_k$  is derived in a standardized way [11, 12], which specifies the base-pair orientation  $\mathbf{R}_k$  and position in space  $\mathbf{p}_k$ , both given relative to some fixed lab frame. The conformation of a piece of DNA is described by the chain  $\mathbf{G} = (\mathbf{g}_1, \mathbf{g}_2, \dots, \mathbf{g}_n)$  of base-pair reference frames. The base-pair *step* conformations are denoted by  $\mathbf{g}_{k+1}$ , i.e. the orientation and position of  $\mathbf{g}_{k+1}$  relative to  $\mathbf{g}_k$ . The data  $\mathbf{R}_k$  and  $\mathbf{p}_k$  may be represented in a number of different coordinate systems, including Euler angles, exponential coordinates, etc. Similarly, the relative step conformations  $\mathbf{g}_{k+1}$  are conventionally discussed in terms of the six base-pair step parameters Tilt, Roll, Twist, Shift, Slide and Rise [13]. At the moment, we avoid fixing a particular coordinate system, considering the frames  $\mathbf{g}_k$  as abstract elements of the rigid motion group.

Unusual DNA conformations can be recognized by their low probabilities in an equilibrium ensemble of freely fluctuating DNA. The corresponding conformational elastic free energy  $A_B(\mathbf{G})$  depends on the base sequence of the chain  $B = b_1 b_2 \dots b_n$ . The free energy  $A_B$

is a potential of mean force which quantifies the strength of deformation of the chain. We fix the zero-point so that  $\min_{\mathbf{G}} A_B = 0$  and call  $A_B$  the elastic energy of the chain as is customary.

We argue that knowledge of the function  $A_B$  can provide valuable information when it is used to derive mean forces<sup>1</sup>: The elastic generalized force by which the chain acts on its  $k$ -th base pair is given by the negative derivative of the chain energy with respect to the  $k$ -th base pair configuration,  $-\mathbf{d}_{\mathbf{g}_k} A_B(\mathbf{G})$ . In the static equilibrium of a DNA-protein complex, this elastic force exerted by DNA is balanced by the *external force* acting on base-pair  $k$

$$\mu_{(k)} = \mathbf{d}_{\mathbf{g}_k} A_B(\mathbf{G}). \quad (2)$$

The basic force balance Eq. 2 allows to infer external forces from DNA conformations. This relation holds for general elastic energy functions, including next-nearest neighbor coupling [14, 15, 16, 17]. However, the best presently available full parameter sets approximate the elastic energy as a sum of harmonic, nearest-neighbor base-pair step energies  $a_{bb'}$  so that

$$A_B(\mathbf{G}) = \sum_{k=1}^{n-1} a_{b_k b_{k+1}}(\mathbf{g}_{kk+1}). \quad (3)$$

For details on our particular choice, see Methods. In this case Eq. 2 specializes to

$$\mu_{(k)} = \mathbf{d}_{\mathbf{g}_k} a_{b_{k-1} b_k}(\mathbf{g}_{k-1k}) + \mathbf{d}_{\mathbf{g}_k} a_{b_k b_{k+1}}(\mathbf{g}_{kk+1}). \quad (4)$$

One sees that the external force on a base-pair  $\mathbf{g}_k$  balances a sum of two terms, which are just the elastic *tensions* in the steps  $k-1, k$  and  $k, k+1$ , respectively.<sup>2</sup> At each end of the chain, there is of course only one-sided tension.

<sup>1</sup>By ‘forces’ we always mean mean forces in the following.

<sup>2</sup>Eq. 4 is the equivalent of the standard relation ‘force = div stress’ of continuum elasticity in the present context of a discrete, linear chain.

Unlike the generalized force itself, the components  $\mu_{(k)i}$  are defined with respect to a particular choice of basis. We pick a basis by requiring that the  $\mu_{(k)i}$  have simple physical interpretations in terms of force and torque.<sup>3</sup> To formulate this idea, we remark that the frames  $\mathbf{g}_k$  are elements of the rigid motion group and can be represented as so-called homogeneous matrices, which are well-known in robotics, see [18]. This approach has been used for coarse-graining the rigid base-pair model [10] and in the context of worm-like chain models of DNA [19]. Here, base-pair frames are written explicitly as  $\mathbf{g}_k = \begin{bmatrix} \mathbf{R}_k & \mathbf{p}_k \\ 0 & 0 & 0 & 1 \end{bmatrix}$  where  $\mathbf{R}_k$  is a  $3 \times 3$  rotation matrix and  $\mathbf{p}_k$  is a  $3 \times 1$  column vector. The base-pair step conformations are calculated as a matrix product  $\mathbf{g}_{kk+1} = \mathbf{g}_k^{-1} \mathbf{g}_{k+1}$  from the base-pair conformations, where  $\mathbf{g}_k^{-1} = \begin{bmatrix} \mathbf{R}_k^T & -\mathbf{R}_k^T \mathbf{p}_k \\ 0 & 0 & 0 & 1 \end{bmatrix}$ . The corresponding matrix generators  $\mathbf{X}_i$  for rotations ( $1 \leq i \leq 3$ ) and translations ( $4 \leq i \leq 6$ ), are  $4 \times 4$  matrices with entries  $(\mathbf{X}_i)_{jk} = \epsilon_{jik} + \delta_{k4} \delta_{i-3j}$ . Using this notation, the derivatives of  $A_B$  with respect to infinitesimal motions of base-pair  $k$ ,

$$\mu_{(k)i} = \left. \frac{d}{dh} \right|_0 A_B(\mathbf{g}_1, \dots, \mathbf{g}_{k-1}, \mathbf{g}_k(\mathbf{1} + h\mathbf{X}_i), \mathbf{g}_{k+1}, \dots, \mathbf{g}_n), \quad (5)$$

have the required simple interpretations:  $(\mu_{(k)i})_{1 \leq i \leq 3}$  are the Cartesian components of the external *torque*  $\mathbf{t}_{(k)}$  on base-pair  $k$  about an axis through  $\mathbf{p}_k$ , while  $(\mu_{(k)i})_{4 \leq i \leq 6}$  are the Cartesian components of the external *force*  $\mathbf{f}_{(k)}$  attacking at  $\mathbf{p}_k$ . These components are relative to the base-pair fixed triad  $\mathbf{R}_k$ . For actually calculating the components Eq. 5, it is convenient to rewrite the step energy  $a_{bb'}$  which is usually given in terms of the rigid base-pair step parameters, in terms of exponential coordinates, see Supplementary Material, Text *supp-1*.

<sup>3</sup>This requirement precludes the use of Euler angles for the orientation  $\mathbf{R}_k$ .

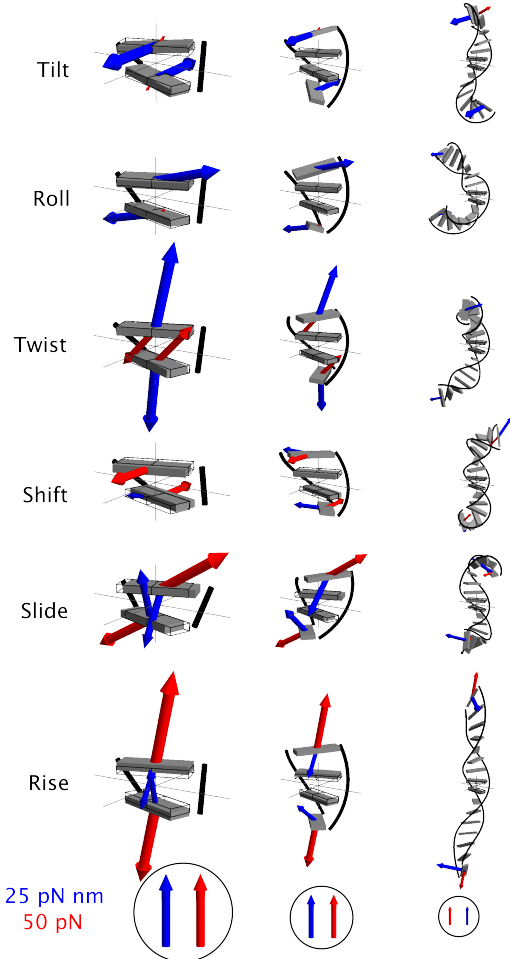


Figure 3: Force and torque pairs acting on DNA to produce an excess of one base-pair step parameter in each row. Torque vectors  $\mathbf{t}_{(1)}, \mathbf{t}_{(2)}$  shown in blue, force vectors  $\mathbf{f}_{(1)}, \mathbf{f}_{(2)}$ , in red. The same deformation of the *central* base-pair step can be produced by external force and torque pairs attacking directly (left column), at the nearest neighbor base-pairs (middle column), or seven base-pairs away (right column). Sequence-averaged MP parameters. For plots of the base-pair step parameters associated with these equilibrium shapes, see Fig. *supp-1*.

An overview of the relation between external forces and torques, and base-pair step deformations is given in Fig. 3. Consider first the left-hand column. The force and torque pairs required for increasing each of the six base-pair step parameters demonstrate the strong coupling between the different base-pair deformation modes of B-form DNA. E.g. to produce pure increased Twist, overwinding torque must be assisted by compressive forces as a consequence of the counter-intuitive twist-stretch coupling [20, 21, 22]. In addition, there exists a geometric coupling effect: Force balance requires that force pairs sum to zero. However, they need not be collinear; any offset of their lines of attack generates an additional torque ‘by leverage’ which enters the torque balance. Thus the external torque vector pairs shown in Fig. 3 do generally not sum to zero.

A base-pair step can be deformed by external forces acting directly on its constituent base-pairs, but also indirectly, by external forces at distant base-pairs. Examples of this non-local effect are shown in the middle and right hand columns of Fig. 3. Here the central base-pair step of each chain has the same deformation as in the left hand column; however this time produced indirectly, by external forces applied only at the chain ends. Along the chain, tensions are non-zero but balanced so that DNA assumes a stressed equilibrium shape [23] in which all intermittent  $\mu_{(k)}$  vanish. These shapes can exhibit strongly non-uniform deformation, e.g. non-uniform Twist, see Fig. *supp-1*. (For a related study of stress localization in RNA, see [24].) Given these complicated shapes, it is difficult to guess at external forces by structural inspection.

In the general case of DNA bound to protein, external forces may act anywhere along the chain. Here each base-pair step deformation is caused by a combination of local external forces and internal propagated tension. In this article, instead of investigating equilib-

rium shapes for given boundary conditions, we focus on the converse question of what local external forces and torques are required for a given general shape. These forces and torques give a quantitative measure for how the proteins forces DNA into that shape.

## Methods

### Rigid base-pair parameter sets

To parametrize the base-pair step energy  $a_{bb'}$ , step equilibrium conformations  $\mathbf{g}_{\text{eq},bb'}$  and stiffness matrices  $\mathbf{S}_{bb'}$  are needed for each dinucleotide type  $bb'$ . We used a combination of knowledge-based and simulation-based parameters. Specifically, the relaxed conformation of each dinucleotide  $bb'$  is the mean conformation reported for  $bb'$  in a crystal structure database of protein-bound DNA fragments [5]. The stiffness matrix  $\mathbf{S}_{bb'}$  for each dinucleotide is the stiffness matrix reported for  $bb'$  as a result of explicit-solvent, all-atom MD simulations of a library of oligonucleotides [4]. We have reported previously on the relation of this hybrid parameter set to pure knowledge-based or pure simulation based parameters [7], and have shown that it reproduces known values  $\mu\text{m}$ -scale elasticity of DNA without fitting [10]. In these articles and here, the hybrid parameter set is denoted by ‘MP’. To evaluate the robustness of our method, we have compared the results computed with MP to those computed with a pure knowledge-based parameter set ‘P’. The P parameter set is essentially identical to the P·DNA parameter set from [5] constructed from mean values and covariance matrices of protein-bound DNA [5], the difference being a global multiplicative factor to correct the temperature scale, see [7]. The dependence of our results on the choice of parameter set is discussed in Results.

### Restrained Relaxation

To account for the high, but limited precision of structural models, we included an initial pre-relaxation stage, a strategy which has been used also for atomistic force fields in related studies [25, 8]. Here, the rigid base pair coordinates of the DNA fragment were allowed to relax simultaneously, descending the gradient of  $A$ ; at the same time, each base-pair was restrained to a region around its original conformation by a sharply increasing potential. We set the size  $r_m$  of this region on the order of the atomic position uncertainty. In this way elastic tension in DNA is allowed to relax, but only so little that the relaxed conformation remains consistent with the reported structural data. The parameter  $r_m$  describes the assumed precision of the input data, and is not a property of the employed force field. To set  $r_m$  we used the estimated coordinate error based on a Luzzati plot as reported in the PDB files if available (which is mostly around 15% of the reported x-ray resolution), and 15% of the resolution otherwise. This gave a range of  $r_m = 0.28 \dots 0.33\text{\AA}$  in the shown examples. The effect of this relaxation on base-pair frame conformations is barely visible by eye, see Fig. 2.

The pre-relaxation procedure can be seen as a form of data smoothing with a tendency to equalize elastic tension in DNA. Force analysis after restrained relaxation produces the set of *smallest* external forces which are compatible with the confidence region of the structural input data. In practice, the effect of relaxation was to reduce extreme peaks in the resulting energy and force profiles, while relaxing the weakest external forces to zero. Thus, relaxation reduces extreme force outliers and eliminates low-level random noise.

Although any sensible choice of  $r_m$  should roughly equal the structural uncertainty, its exact value remains undetermined. The global

scale of our computed forces and torques depends on the value of  $r_m$ , but their relative magnitudes along the chain and their directions are only weakly affected by this choice. After relaxation, we also found substantially increased agreement between energies and forces computed using different elastic parameter sets. These features of pre-relaxation are illustrated by Fig. *supp-2*.

### Implementation and Visualization

Forces and torques in this article were computed starting from the following Protein Data Bank [26] high-resolution structures: *1nvp*, *1cdw*, *1qne* for TBP, *1l1m* for lac repressor and *1cz0* for *Ippp*-I. Rigid base-pair frames were computed from atomic coordinates by least-squares fitting of model base-pairs following a standardized procedure, using the 3DNA program [11, 12]. Calculation of energies, forces and torques as described in section DNA nano-mechanics, as well as pre-relaxation were implemented in Mathematica. Three-dimensional vector depictions of base-pair conformations, forces and torques were exported as VRML files, which are available as Supplementary Material Data S1-S3. They can be visualized and superimposed with atomic structure data using molecular visualization software, for instance the free molecular visualization program Chimera [27] which was used for the images in this article.

## Results

We have applied an analysis as described above for three x-ray co-crystal structures of TATA-box binding protein [28, 29, 30] and an ensemble of 20 NMR solution structure conformers of a lac repressor complex [31]. As an example of a trapped intermediate state of a structural modification of DNA, we analyzed a co-crystal structure of the homing endonuclease

*I-ppoI* [32].

Fig. 4 illustrates the force analysis of TATA-box binding protein (TBP) complexed with cognate DNA. In this complex, TBP bends DNA into the major groove. The overall turn of about  $80^\circ$  is distributed over the eight base-pairs of the TATA-box, whose steps have uniform positive roll. The highest deformation energy occurs at the first ‘TA’ dinucleotide step whose base-pairs (9 and 10) are separated but not strongly kinked. A secondary peak in elastic energy can be seen at base-pair step 15-16. Inspection of the structure shows that at both of these locations, a phenylalanine residue partially intercalates between the base-pairs. The initial, straight poly-G DNA region shows only small deformation energies.

Superimposed on the TFIIA-TBP-DNA crystal structure [30], Fig. 4 shows force and torque vectors from an analysis of three different co-crystals of TBP with the same DNA binding site. A strong opposing force pair is seen to pull apart base-pairs 9 and 10. Along the box, the  $80^\circ$  turn is associated with a nicely aligned sequence of torque vectors at base-pairs 10 to 15; they deviate by at most  $28^\circ$  from pointing into the major groove. Unlike the rather evenly distributed torques, the base-pair forces have a minimum in the center of the box, and a second peak associated with a force pair stretching the base-pair step 15-16. Note that the directions of forces and torques at base-pairs 9-10 and 15-16 are approximately related by a two-fold symmetry around step 12-13 corresponding to the symmetry of TBP; however their magnitudes are about half at base-pairs 12-13. Base-pairs 1-8 are present in only one of the crystal structures, and exhibit low force and torque magnitudes

Fig. 5 shows the nano-mechanics analysis of an NMR solution structure ensemble of *E. coli* lac repressor bound to DNA. In this complex, a wild-type operator with non-palindromic sequence is bound by a homodimer of the lac re-

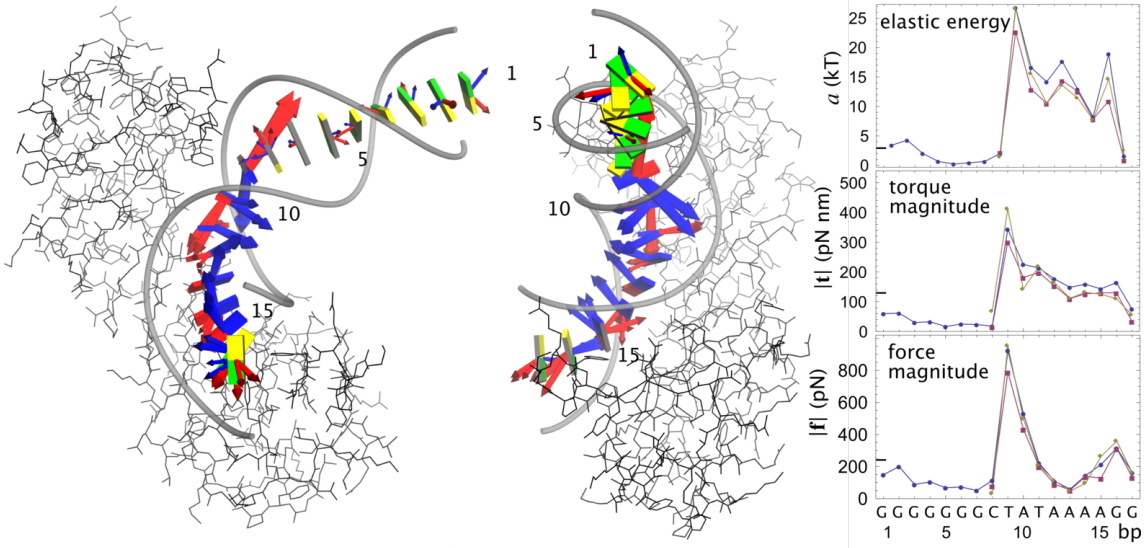


Figure 4: TFIIA(not shown)-TBP-DNA complex with force and torque vectors from three different TBP-DNA crystal structures, left. Corresponding energy, force magnitude and torque magnitude profiles, right. Here and in the following figures, linear forces  $\mathbf{f}_{(k)}$  are shown as red arrows, torques  $\mathbf{t}_{(k)}$  as blue arrows; base-pairs are represented as numbered small boxes with sequence coloring, ‘A’ red, ‘T’ blue, ‘G’ green, ‘C’ yellow; the two viewpoints are rotated by  $90^\circ$  around the vertical axis. Sequence (5’, base-pair 1)-GGGGGGGGCTATAAAAGG-(3’, base-pair 17). Allowed relaxation range  $r_m = 0.3\text{\AA}$  in all complexes. MP parameter set. The three-dimensional representations of base-pairs, force and torque vectors used for this figure are available, as detailed in Methods (Supplementary Material, Data S1).

pressor DNA binding domain [31]. The resulting complex structure is only approximately two-fold symmetric. The strongest deformations occur around the central six base-pairs 9-14, producing the overall  $30^\circ$  bend of DNA. The kink at the symmetry center 11-12 has by far the highest elastic energy.

As in the TBP case, the peak of elastic energy is associated with a pair of base-pair stretching forces, here accompanied by a strong unwinding torque pair. In the central region 9-14, force and torque directions closely follow the approximate two-fold symmetry of the complex, despite the fact that the sequence is asymmetric. Outside the central region, force and torque symmetry is broken. Secondary peaks in torque and force magnitude can be

identified at the symmetry-related base-pair steps 6-7 and 16-17. At base-pairs 6 and 7, a rather weak pair of shearing forces attack, while base-pairs 16 and 17 are pulled apart by a strong stretching force pair. Also, a strong torque on base-pair 19 has no counterpart at the symmetry-related position 4, highlighting the different binding modes of the two half-sites.

Fig. 6 illustrates the analysis of the homing endonuclease *Ippo-I*, bound to target DNA substrate in an un-cut state. This complex has a palindromic operator sequence and an overall two-fold symmetry. Cleavage occurs within at step 8-9 (and the symmetry-related 12-13) in the active form of the complex. In contrast to lac, deformation of the operator occurs mainly



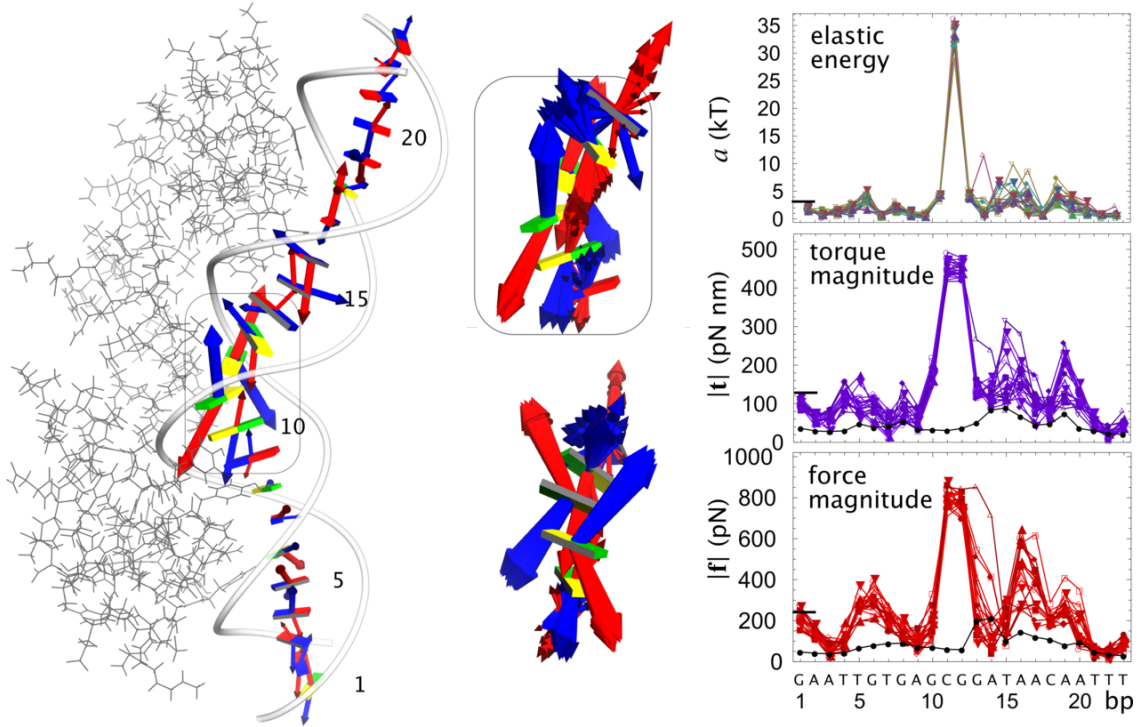


Figure 5: Complex of lac repressor and DNA. NMR structure of one out of 20 conformers with ensemble mean force and torque vectors, left. Two magnified views of the encircled region, middle column, with force and torque vectors of all conformers. Ensemble energy, torque and force magnitude profiles, right; the ensemble standard deviation profiles  $\langle |\mathbf{f}_{(k)}|^2 \rangle_{\text{NMR}}^{1/2}$  and  $\langle |\mathbf{t}_{(k)}|^2 \rangle_{\text{NMR}}^{1/2}$  of force and torque vectors are shown in black. MP parameter set. Sequence (5', base-pair 1)-GAATTGTGAGCGGATAACAATTT-(3', base-pair 23). The three-dimensional representations in Data S2.

not at the symmetry center 10-11 but within the triplet 7-8-9 (12-13-14). The intervening base-pair steps are sheared and tilted, producing the overall  $45^\circ$  bend of the binding site.

The computed external forces show that these deformation are mainly due to a pair of strong opposing forces attacking at base-pairs 7 and 9 (12 and 14), stretching and shearing the triplets. In addition, there is an external torque attacking at the intermediate base-pair 8 (13). While the adjacent base-pair step 9-10 (11-12) is almost completely relaxed, the central step is sheared by an opposing lateral force pair.

## Discussion

We point out the main general features of an analysis of DNA-protein complex structures in terms of base-pair forces and torques, using the structures presented in the Results section as examples.

### Robustness of nano-mechanics analysis

The conformational data on which our analysis is based, as well as the elastic parameter sets, are reliable within certain bounds of error.

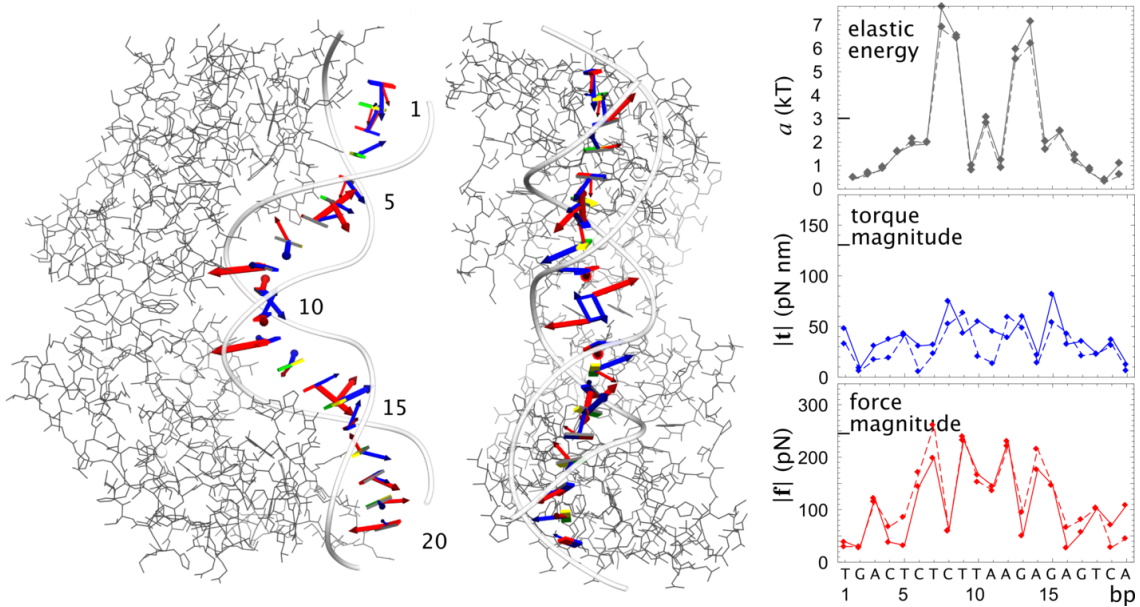


Figure 6: *Ippo-I* DNA complex. The points of single-strand cuts in the functional complex are indicated. Relaxation range  $r_m = 0.3\text{\AA}$ . The MP parameter set was used for vectors, and MP (solid line) and P (dashed line) parameter sets for profiles, right. Sequence (5', base-pair 1)-TGACTCTCTT·AAGAGAGTCA-(3', base-pair 20). Three-dimensional representations in Data S3.

How do these sources of uncertainty influence the derived external forces and torques?

To assess the dependence on details of crystallization, we computed forces and torques based on three x-ray structures of the TBP complex, see Fig. 4. Two of the complexes lack TFIIA and all three crystals have different space groups and thus different crystal contacts. Nonetheless, their energy, force and torque profiles quantitatively agree at common base-pairs. As can be seen from the three-dimensional representation, also force and torque directions agree closely.

The conformational variability within an NMR structure ensemble leads to variability of elastic energies, external forces and torques. These were computed for a lowest-energy ensemble of 20 conformers of the lac repressor solution structure [31], see Fig. 5. We find that the main features of the corresponding profiles

are clearly more pronounced than the variation across the ensemble. Also forces and torque directions are robust among conformers, with the exception of the most weakly forced base-pairs.

When comparing computed forces and torques corresponding to the different parameter sets P and MP, we find surprisingly good agreement (Fig. 6), considering the completely different sources (crystal structure database for P, MD simulation for MP, see Methods) of the stiffness parameters.

The choice of pre-relaxation range  $r_m$  reflects the assumed precision of the structural input. It does not strongly affect the relative magnitudes of local forces and torques. However a present limitation of the method comes from the fact that overall force and torque scales vary with  $r_m$ . Setting  $r_m$  to the structural precision, leads to the lowest external forces that are compatible with the considered struc-

tural model. While this choice is reasonable, it could be improved upon by incorporating information on the equilibrium fluctuations of bound base-pairs derived from the local B-factors. Clearly, a direct comparison to averaged forces from full simulations of protein-DNA complexes would be enlightening. Note however that compared to the construction of hybrid base-pair potentials [7], the correction of known artifacts such as systematic undertwist is less straightforward for atomic force fields.

### Force scale and validity range

The characteristic scales of base-pair forces and torques in thermal equilibrium at room temperature are determined by equipartition of energy. They result as 245 pN and 130 pN nm, respectively. (For base-pair step tensions one obtains 170 pN and 90 pN nm.) Thus in a thermal equilibrium ensemble, the instantaneous forces of a harmonic base-pair step are normally distributed with width 245 pN, so that on average 10 % of instantaneous forces are higher than 400 pN. We conclude that our elastic potentials are well supported by MD simulation up to around 400 pN and 200 pN nm.

In our examples, only a few of the highest force peaks exceed that range. This can be expected also for most other complexes: In the DNA-protein crystal structure database [5], the bulk of DNA base-pair steps was slightly *less* deformed [7] than in the thermal ensemble [4]. Note however that outlying base-pair steps do occur in the crystal database; they are preferentially deformed into the softest directions [5]. Together with the observation of unexpectedly frequent sharp bending of DNA [33] this suggests that the true free energy function stays below the harmonic approximation for strong deformations, cf. Fig.1. Thus forces and torques tend to be overestimated outside the validity range given above.

Our force field is parametrized by MD simu-

lations at room temperature, while the crystal structures are typically observed at  $\simeq 110$  K. The computed forces are thus predictions for the complex at room temperature under the assumption that the mean conformation is essentially the same as at 110 K. This assumption is ubiquitous in structural biology when interpreting crystal structures in terms of biological function. On the other hand, we cannot assume that the mean conformation from the crystal, or the force field, are valid at temperatures that approach the melting temperature of DNA. Not only will the increased thermal fluctuations exceed harmonic range of the potential described above. Also, the stiffness parameters themselves change with temperature due to the entropic part contained in the elastic free energy. Finally, the basic requirement of the rigid base-pair model that internal degrees of freedom are uncoupled between neighboring base-pairs is violated by cooperative base-pair opening. As a result, it is hard to estimate the temperature range of validity of the present force calculation. A very loose upper bound is  $\simeq 330$  K where local bubble formation starts.

The limitations listed above arise from the presently available free energy functions; the general procedure of force and torque extraction is unchanged for general anharmonic free energies, or free energies that include inter-base degrees of freedom.

### Protein forces may exceed critical forces for DNA structural transitions

Even though within thermal range, forces of hundreds of pN may appear unreasonable given that typical critical forces and torques for disrupting B-DNA structure in single-molecule experiments are only  $f_c \simeq 65$  pN and  $t_c \simeq 40$  pN nm [34], and that unzipping occurs already at  $\simeq 15$  pN. To see that there is in fact no contradiction, note the qualitative difference between protein forces acting lo-

cally on B-DNA, and externally applied micro-manipulation forces. Consider again the stereotypical double-well free energy in Fig. 1, where the potential wells at  $x_1$  and  $x_2$  could for example correspond to B-DNA and to an overstretched state (S-DNA), respectively. Without external force, the ground state is  $x_1$ . A protein which binds DNA constrains the base-pair step to a position  $x_d$  close to  $x_1$ . The required mean force is  $f_d = A'(x_d)$ ; it is entirely determined by the local potential well. On the other hand, an external force  $f$  pulling on the DNA fragment acts by tilting the free energy landscape, such that eventually  $x_2$  becomes the ground state. The critical external force  $f_c = \Delta A/\Delta x$  for the transition is determined by the free energy difference between the potential wells and their separation, independent of local well steepness. Thus for steep but nearly degenerate and well separated potential minima, one gets  $f_d > f_c$  for moderate displacements  $x_d - x_1$ . Entropic effects have been neglected; they add minor corrections.

In the example of the overstretching transition, the critical force is  $f_c \simeq 65$  pN [34]. The stiffness and thermal standard deviation of base-pair elongation are  $k_1 \simeq 10k_B T/\text{\AA}^2$  and  $0.33$  \AA, respectively [10]. Thus, stretching the base-pair step by one standard deviation already requires twice the critical force (and  $4f_c$  if the next step is compressed by the same amount).

### Sharp elastic energy peaks result from balanced pairs of force and torque

The elastic energy gives a scalar measure of the overall deviation of each base-pair step from its equilibrium conformation. Elastic energy profiles can therefore quickly show the hot spots of local deformation of complexed DNA. A recurring motif in the analyzed profiles is an isolated high energy peak flanked by low energy steps. The energy peak motif generally indi-

cates a force and torque *pair* deforming the high-energy step, which approximately satisfies a local force and torque balance. An example is provided by base-pair step 11-12 in the lac repressor (Fig. 5). The three-dimensional force and torque vectors show that this step is kinked by opposing pairs of force and torque with stretching, shearing and underwinding components. Further examples with less complete balance is presented by the stretching force pair at base-pairs 9 and 10 in TBP (Fig. 4), and by the more weakly deformed, symmetry-related step 15-16.

### Directions of deformation and force are non-trivially related

Force and torque vectors often do not point into the directions one would expect when picturing DNA as made up from some uniform isotropic elastic material. This non-intuitive feature is visible in Fig. 3 but occurs also in force analyses of complex structures.

For example, regarding the forces needed to produce the  $80^\circ$  turn in TBP (Fig. 4) one may have two non-exclusive naive expectations: two point forces could push the ends of the curved region at base-pairs 9 and 16 towards the center of the circle of curvature, compensated by a force pulling the center of the curved region away from this point; or distributed torques along the curved region could try to bend DNA into the major groove, their torque vectors pointing normal to the local plane of bending, i.e. towards one of the backbones. The computed forces and torques prove both of these expectations wrong. Clearly all forces observed in the complex point roughly along the local helical axis, not perpendicular to it; and distributed torques do occur but point into the major groove, at right angles to the expected direction. Thus, the coupled mechanical properties of DNA produce the observed  $80^\circ$  turn of the TATA box by an array

of torques as would result, from pulling both sugar-phosphate backbones into the respective 3' direction. Interestingly, in an MD simulation of a TATA sequence without protein [35], this mode of external 3'-pulling was observed to produce a bent shape that mimics the bound conformation of DNA in the complex.

Another example of this coupling is the 36° Roll of the base-pair step 9-10 of the lac repressor complex. As can be seen in Fig. 5, it results not from a bending torque but mainly from stretching and underwinding by the protein. In summary, the non-trivial nano-mechanical properties of DNA make it impossible to tell by eye what force and torque directions are required for a particular shape.

### **Forces require DNA-protein contacts, but contacts do not always transmit force**

In the absence of long-range interactions, only base-pairs that are contacted by protein should ever experience external forces. The converse is not true: not every contact can be expected to actually transmit force. These requirements allow for a consistency check of a DNA nano-mechanics analysis by comparing calculated external forces with observed contact points. For example, in the lac repressor, base-pairs 2, 3, 21 and 22 are non-contacted, and indeed their forces and torques are weak. The remaining magnitude gives an estimate of the error in force determination of about 10% of the peak force. This error estimate agrees with the standard deviation of forces and torques across the NMR ensemble, cf. Fig. 5. We conclude that possible systematic errors in force determination are smaller than the uncertainty due to limited structural precision. In contrast, the calculated forces and torques at the non-contacted end base-pairs 1 and 23 of the binding site are about three times the error estimate. Their non-zero forces point to a sys-

tematic error, possibly due to the dissimilar properties of internal and end base-pairs, see Methods. Base-pair 9 in the same complex is an example of a base-pair in close contact with protein residues which experiences forces indistinguishable from 0, showing that contacts do not imply local forcing.

A similar situation can be found in the TBP repressor complex [30], Fig. 4. Here the boundary base-pairs 1 and 2 are contacted by protein from a neighboring unit cell, not shown in Fig. 4, and are therefore not expected to be free. In contrast base-pairs 3 to 7 represent a stretch of suspended, non-contacted poly-G DNA and are expected to be force-free. Indeed their residual force and torque magnitudes are only about 20% of the thermal force scale; this margin can serve as an error estimate.

### **DNA is deformed by a combination of local forces and propagated tension**

Apart from local forces, tension from flanking DNA can deform a base-pair step, see Fig. 3. A well-known extreme example of tension propagation is the lac operon, where a tight loop of many base-pairs is held together by two copies of the lac repressor dimer [36, 37, 38, 39]. While forces are exerted only at the ends, the propagated tension deforms DNA along the loop. In protein-DNA complexes, the observed deformations of bound DNA are generally due to the combination of local external forces and torques and distant forces and torques, propagated as tension along the chain. This non-local part is always present when forces do not balance locally, but becomes most apparent when deformations occur without local forces. Considering base-pairs 7-9 in the *Ippo-I* complex, Fig. 6, note that both steps 7-8 and 8-9 are stressed as indicated by their high elastic energy. However base-pair 8 in the middle experiences only weak external force. This motif can be interpreted mechanically as follows:

The protein pulls base-pairs 7 and 9 apart by a nearly antiparallel force-pair leaving base-pair 8 suspended freely in the middle. Interestingly, the single strand cuts performed by the functional form of the *Ippo-I* complex occur exactly at the pre-stretched base-pair step 8-9 and the symmetry-related site 12-13.

## Conclusions

In this article we have presented an analysis of DNA nano-mechanics within a given complex structure as a novel but natural way to think about the interaction of DNA with proteins. The free energy function of any coarse-grained model allows calculation of the mean forces acting on the represented degrees of freedom. Our basic idea is to infer these mean forces from structural data and use them to describe the mechanical interaction of DNA with its environment. This gives an intuitive way to interpret the mechanics of DNA-protein binding, augmenting the interpretation of molecular conformation.

We have implemented this idea for the rigid base-pair model of DNA, using an efficient and compact matrix formalism to derive the forces and torques acting on base-pairs. This level of coarse-graining offers good compromise between resolution and reliability. In particular, the available parameter sets summarize comprehensive structure database analysis and large-scale MD simulation efforts. Our method puts this large body of DNA elasticity to work in a computationally inexpensive way. As we have demonstrated, the results are robust with respect to differences in crystallization and among conformers in an NMR structure ensemble, force profiles using different parameter sets converge after pre-relaxation, and forces on non-contacted base-pairs vanish within the estimated error bounds. New, nonlinear or poly-nucleotide potentials will lead to improved

accuracy and range of applicability of nano-mechanics analysis.

From a physical chemistry point of view, base-pair forces and torques are interesting in their own right since they describe the intermolecular force balance. They are easy to interpret since they are local quantities. However, they are *not* easy to deduce from a structure ‘by eye’, since they depend non-locally on DNA deformation, by propagation of elastic tension. Thus while it only takes a crystal structure as input, DNA nano-mechanics analysis can improve on pure conformation analysis by integrating prior knowledge about DNA elasticity.

To predict indirect readout effects, i.e. sequence specificity of proteins mediated by DNA elasticity and structure, it is desirable to calculate the elastic contributions to protein-DNA binding free energies, see e.g. [7]. Nano-mechanics analysis is not directly useful for this purpose, since energies can be calculated directly from the deformations. However, good estimates for the total elastic energy of a protein-DNA complex require some elastic model of the protein. Comparison of predicted and structure-based base-pair forces appears a good way to validate such coarse-grained protein models.

A related application of our method is to establish a connection between multi-scale biomolecular simulation and experimental structural data. Common simulation schemes connect different levels of coarse-graining by force-matching [40, 41]. Simulated and structure-based base-pair forces can be matched with little extra effort, suggesting a data-driven method for the rational design and validation of new coarse-grained protein models. Our analysis also establishes a link between structural studies and biophysical force measurements on short DNA loops [42].

From a biochemistry point of view, interpretation of structures in terms of interac-

tion forces leads to hypotheses about their biological functioning. For instance, DNA-modifying proteins such as nucleases inflict strong DNA deformations; when trapped intermediate states can be crystallized, their base-pair interaction forces shed light on the reaction mechanism, see the *Ippo-I* example in Results. Furthermore, the strength of transmitted force constitutes a measure to classify local sites of interaction, as applied in a related article on nucleosome nano-mechanics [43]. The strongest-force contacts play the most important role in enforcing the structural constraints implied by binding. Thus, mutation of a DNA base or a protein residue affecting a high-force contact site is expected to result in strong perturbation of the complex structure, while small-force contacts should only weakly affect the global structure of the complex. So whenever the global DNA conformation on a scale of several base-pairs is relevant for biological function of a complex, high-force contact sites emerge as natural targets for mutation assays. We refer the reader to [43] for a first observation of the effect of mutations on the force patterns.

## Acknowledgment

This work was supported by the chair of excellence program of the Agence Nationale de la Recherche (ANR). The authors wish to thank R. Lavery for helpful discussion.

## References

- [1] H. G. Garcia, P. Grayson, L. Han, M. Inamdar, J. Kondev, P. C. Nelson, R. Phillips, J. Widom, and P. A. Wiggins. Biological consequences of tightly bent dna: the other life of a macromolecular celebrity. *Biopolymers*, 85(2):115–30, 2007.
- [2] Timothy J Richmond and Curt A Davey. The structure of DNA in the nucleosome core. *Nature*, 423(6936):145–150, 2003.
- [3] C.R. Calladine. Mechanics of sequence-dependent stacking of bases in B-DNA. *J Mol Biol*, 161(2):343–52, 1982.
- [4] F. Lankaš, J. Šponer, J. Langowski, and T.E. Cheatham, 3rd. DNA basepair step deformability inferred from molecular dynamics simulations. *Biophys J*, 85(5):2872–83, 2003.
- [5] W.K. Olson, A.A. Gorin, X.J. Lu, L.M. Hock, and V.B. Zhurkin. DNA sequence-dependent deformability deduced from protein-DNA crystal complexes. *Proc Natl Acad Sci U S A*, 95(19):11163–8, 1998.
- [6] S. Ahmad, H. Kono, M.J. Arauzo-Bravo, and A. Sarai. ReadOut: structure-based calculation of direct and indirect readout energies and specificities for protein-DNA recognition. *Nucleic Acids Res*, 34(Web Server issue):W124–7, 2006.
- [7] Nils B Becker, Lars Wolff, and Ralf Everaers. Indirect readout: detection of optimized subsequences and calculation of relative binding affinities using different dna elastic potentials. *Nucleic Acids Res*, 34(19):5638–5649, 2006.
- [8] A.V. Morozov, J.J. Havranek, D. Baker, and E.D. Siggia. Protein-DNA binding specificity predictions with structural models. *Nucleic Acids Res*, 33(18):5781–98, 2005.
- [9] N.R. Steffen, S.D. Murphy, L. Toller, G.W. Hatfield, and R.H. Lathrop. DNA sequence and structure: direct and indirect recognition in protein-DNA binding. *Bioinformatics*, 18 Suppl 1:S22–30, 2002.
- [10] Nils B. Becker and Ralf Everaers. From rigid base pairs to semiflexible polymers: Coarse-graining dna. *Physical Review E (Statistical, Nonlinear, and Soft Matter Physics)*, 76(2):021923, 2007.
- [11] W. K. Olson, M. Bansal, S. K. Burley, R. E. Dickerson, M. Gerstein, S. C. Harvey, U. Heinemann, X. J. Lu, S. Neidle, Z. Shakked, H. Sklenar, M. Suzuki, C. S. Tung, E. Westhof, C. Wolberger, and H. M. Berman. A standard reference frame for the description of nucleic acid base-pair geometry. *J Mol Biol*, 313(1):229–37, 2001.
- [12] X. J. Lu and W. K. Olson. 3DNA: a software package for the analysis, rebuilding and visualization of three-dimensional nucleic acid structures. *Nucleic Acids Res*, 31(17):5108–21, 2003.
- [13] R.E. Dickerson. Definitions and nomenclature of nucleic acid structure components. *Nucleic Acids Res*, 17(5):1797–803, 1989.
- [14] K Yanagi, G G Prive, and R E Dickerson. Analysis of local helix geometry in three b-dna decamers and eight dodecamers. *J Mol Biol*, 217(1):201–214, 1991 Jan 5.
- [15] M J Packer, M P Dauncey, and C A Hunter. Sequence-dependent dna structure: tetranucleotide conformational maps. *J Mol Biol*, 295(1):85–103, 2000 Jan 7.



- [16] D.L. Beveridge, G. Barreiro, K.S. Byun, D.A. Case, T.E. Cheatham, 3rd, S.B. Dixit, E. Giudice, F. Lankas, R. Lavery, J.H. Maddocks, R. Osman, E. Seibert, H. Sklenar, G. Stoll, K.M. Thayer, P. Varnai, and M.A. Young. Molecular dynamics simulations of the 136 unique tetranucleotide sequences of DNA oligonucleotides. I. Research design and results on d(CpG) steps. *Biophys J*, 87(6):3799–813, 2004.
- [17] Satoshi Fujii, Hidetoshi Kono, Shigeori Takenaka, Nobuhiro Go, and Akinori Sarai. Sequence-dependent dna deformability studied using molecular dynamics simulations. *Nucleic Acids Res*, 35(18):6063–6074, 2007.
- [18] R.M. Murray, Z. Li, and S.S. Sastry. *A mathematical introduction to robotic manipulation*. CRC Press, Boca Raton, 1993.
- [19] G. S. Chirikjian and Y. F. Wang. Conformational statistics of stiff macromolecules as solutions to partial differential equations on the rotation and motion groups. *Physical Review E*, 62(1):880–892, 2000.
- [20] T. Lionnet and F. Lankas. Sequence-dependent twist-stretch coupling in dna. *Biophys J*, 92(4):L30–2, 2007.
- [21] T. Lionnet, S. Joubaud, R. Lavery, D. Bensimon, and V. Croquette. Wringing out DNA. *Phys Rev Lett*, 96(17):178102, 2006.
- [22] J. Gore, Z. Bryant, M. Nollmann, M. U. Le, N. R. Cozzarelli, and C. Bustamante. DNA overwinds when stretched. *Nature*, 442(7104):836 – 839, AUG 17 2006.
- [23] B. D. Coleman, W. K. Olson, and D. Swigon. Theory of sequence-dependent DNA elasticity. *Journal of Chemical Physics*, 118(15):7127–7140, 2003.
- [24] A Fernandez. Stress localization in the rna backbone: a mechanical footprint for predicting base-backbone tertiary contacts. *J Theor Biol*, 166(4):443–452, 1994.
- [25] G. Paillard and R. Lavery. Analyzing protein-DNA recognition mechanisms. *Structure*, 12(1):113–22, 2004.
- [26] F C Bernstein, T F Koetzle, G J Williams, E F Jr Meyer, M D Brice, J R Rodgers, O Kennard, T Shimanouchi, and M Tasumi. The protein data bank: a computer-based archival file for macromolecular structures. *J Mol Biol*, 112(3):535–542, 1977.
- [27] E.F. Pettersen, T.D. Goddard, C.C. Huang, G.S. Couch, D.M. Greenblatt, E.C. Meng, and T.E. Ferrin. Ucsf chimera - a visualization system for exploratory research and analysis. *J. Comput. Chem.*, 25(13):1605–1612, 2004.
- [28] D B Nikolov, H Chen, E D Halay, A Hoffman, R G Roeder, and S K Burley. Crystal structure of a human tata box-binding protein/tata element complex. *Proc Natl Acad Sci U S A*, 93(10):4862–4867, 1996.
- [29] G A Patikoglou, J L Kim, L Sun, S H Yang, T Kodadek, and S K Burley. Tata element recognition by the tata box-binding protein has been conserved throughout evolution. *Genes Dev*, 13(24):3217–3230, 1999.
- [30] Michael Bleichenbacher, Song Tan, and Timothy J Richmond. Novel interactions between the components of human and yeast tfiia/tbp/dna complexes. *J Mol Biol*, 332(4):783–793, 2003.
- [31] Charalampos G Kalodimos, Alexandre M J J Bonvin, Roberto K Salinas, Rainer Wechselberger, Rolf Boelens, and Robert

- Kaptein. Plasticity in protein-dna recognition: lac repressor interacts with its natural operator O1 through alternative conformations of its dna-binding domain. *EMBO J*, 21(12):2866–2876, 2002.
- [32] E. A. Galburt, B. Chevalier, W. Tang, M. S. Jurica, K. E. Flick, R. J. Monnat, Jr, and B. L. Stoddard. A novel endonuclease mechanism directly visualized for i-ppoi. *Nat Struct Biol*, 6(12):1096–9, 1999.
- [33] P. A. Wiggins, T. van der Heijden, F. Moreno-Herrero, A. Spakowitz, R. Phillips, J. Widom, C. Dekker, and P. C. Nelson. High flexibility of DNA on short length scales probed by atomic force microscopy. *Nat Nano*, 1:137–141, 2006.
- [34] Abhijit Sarkar, Jean-Francois Leger, Didier Chatenay, and John F. Marko. Structural transitions in DNA driven by external force and torque. *Physical Review E (Statistical, Nonlinear, and Soft Matter Physics)*, 63(5):051903, 2001.
- [35] D Flatters, M Young, D L Beveridge, and R Lavery. Conformational properties of the tata-box binding sequence of dna. *J Biomol Struct Dyn*, 14(6):757–765, 1997.
- [36] M C Mossing and M T Jr Record. Upstream operators enhance repression of the lac promoter. *Science*, 233(4766):889–892, 1986.
- [37] H Kramer, M Niemoller, M Amouyal, B Revet, B von Wilcken-Bergmann, and B Muller-Hill. lac repressor forms loops with linear dna carrying two suitably spaced lac operators. *EMBO J*, 6(5):1481–1491, 1987.
- [38] Yongli Zhang, Abbye E McEwen, Donald M Crothers, and Stephen D Levene. Analysis of in-vivo lac-mediated gene repression based on the mechanics of dna looping. *PLoS ONE*, 1:e136, 2006.
- [39] David Swigon, Bernard D Coleman, and Wilma K Olson. Modeling the lac repressor-operator assembly: the influence of dna looping on lac repressor conformation. *Proc Natl Acad Sci U S A*, 103(26):9879–9884, 2006.
- [40] Sergei Izvekov and Gregory A Voth. A multiscale coarse-graining method for biomolecular systems. *J Phys Chem B*, 109(7):2469–2473, 2005 Feb 24.
- [41] Gary S Ayton, Will G Noid, and Gregory A Voth. Multiscale modeling of biomolecular systems: in serial and in parallel. *Curr Opin Struct Biol*, 17(2):192–198, 2007 Apr.
- [42] Hari Shroff, David Sivak, Jake J Siegel, A L McEvoy, Merek Siu, Andrew Spakowitz, Phillip L Geissler, and Jan Liphardt. Optical measurement of mechanical forces inside short dna loops. *Biophys J*, 94(6):2179–2186, 2008.
- [43] N.B. Becker and R. Everaers. DNA nanomechanics in the nucleosome. *under review, manuscript included in this submission*, 2008.
- [44] Y. Shi, S. He, and J.E. Hearst. Statistical mechanics of the extensible and shearable elastic rod and of DNA. *J. Chem. Phys.*, 105(2):714–31, 1996.

*DNA nano-mechanics*

**Supplementary figures and text**

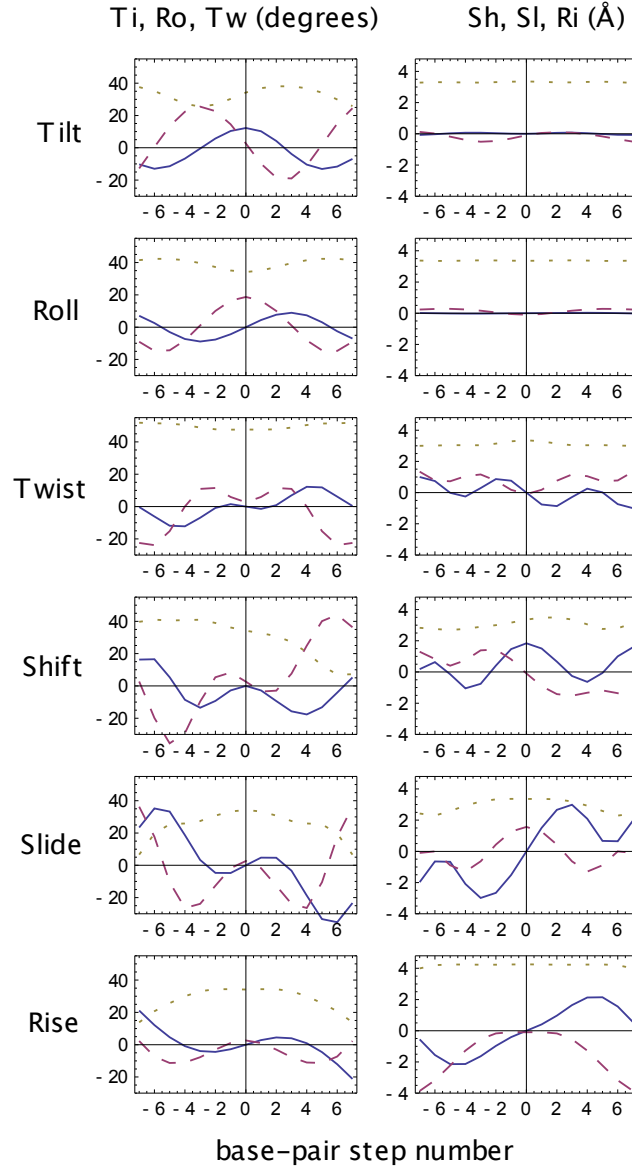


Figure *supp-1*: Tilt, Roll, Twist (left column) and Shift, Slide, Rise (right column) base-pair parameters corresponding to the equilibrium shapes of homogeneous DNA shown in the rightmost column of Fig. 3. Tilt and Shift, solid line; Roll and Slide, dashed; Twist and Rise, dotted. At the central base-pair step 0, all parameters except for the perturbed one, are at their equilibrium values in each row. One can see that unlike the case of a shearable rod with uncoupled modes and isotropic bending [44], the excess twist is *not* constant. As a consequence, external forces acting in non-equilibrium shapes cannot be deduced directly from local excess base-pair parameter values. Due to DNA symmetry properties, the two halves of the chain with positive and negative bp are identical only in the Roll, Twist, Slide and Rise panels. In these panels, the excess base-pair step parameters exhibit (anti)-symmetric profiles. The elastic energy (not shown) also varies along the chain.

**Text *supp-1* Base-pair step potentials in exponential coordinates**

We parametrize a base-pair step conformation  $\mathbf{g}_{kk+1}$  by letting

$$\mathbf{g}_{kk+1} = \mathbf{g}_{\text{eq},b_k b_{k+1}} \exp[q_{kk+1}^j \mathbf{X}_j] \quad (\text{supp-1})$$

where  $\exp$  is the matrix exponential and  $\mathbf{g}_{\text{eq},b_k b_{k+1}}$  is the equilibrium base-pair step conformation. That is, step conformations are given in exponential coordinates on the rigid motion group, based at the point  $\mathbf{g}_{\text{eq},b_k b_{k+1}}$  [10]. The harmonic step energy function can be written as

$$a_{bb'}(\mathbf{g}_{kk+1}) = \frac{1}{2} q_{kk+1}^i \mathbf{S}_{(b_k b_{k+1})ij} q_{kk+1}^j, \quad (\text{supp-2})$$

where  $\mathbf{S}$  can be obtained from stiffness matrices given in base-pair step parameters by multiplying with appropriate Jacobian matrices. In the coordinates introduced above, the external forces have simple expressions for weakly deformed steps. One obtains to first order,

$$\mu_{(k)i} = \mathbf{S}_{(b_{k-1} b_k)ij} q_{k-1k}^j - (\mathbf{A}_{kk+1}^\top \mathbf{S}_{(b_{k-1} b_k)})_{ij} q_{kk+1}^j + O(q)^2, \quad (\text{supp-3})$$

where  $\mathbf{A}_{kk+1} = \mathbf{Ad}(\mathbf{g}_{\text{eq},b_k b_{k+1}})$  and  $\mathbf{Ad}$  denotes the adjoint representation of the group; for details, see [10]. For base-pair steps that are deformed more strongly, it was necessary to consider the corrections to this first order result. We therefore postulated the quadratic energy Eq. *supp-2* to be valid for finite extensions, and recovered  $\mu_{(k)i}$  by using the Jacobian matrix  $\mathbf{J}_{\text{exp}}$  relating exponential coordinates to the left invariant frame; one then gets

$$\mu_{(k)i} = (\mathbf{J}_{\text{exp}}^\top(q_{k-1k}) \mathbf{S}_{(b_{k-1} b_k)})_{ij} q_{k-1k}^j - (\mathbf{A}_{kk+1}^\top \mathbf{J}_{\text{exp}}^\top(q_{kk+1}) \mathbf{S}_{(b_k b_{k+1})})_{ij} q_{kk+1}^j. \quad (\text{supp-4})$$

Here, the Jacobian is given by  $\mathbf{J}_{\text{exp}}^{-1}(q) = \int_0^1 \mathbf{Ad}(\exp(-s q^i \mathbf{X}_i)) ds$ .

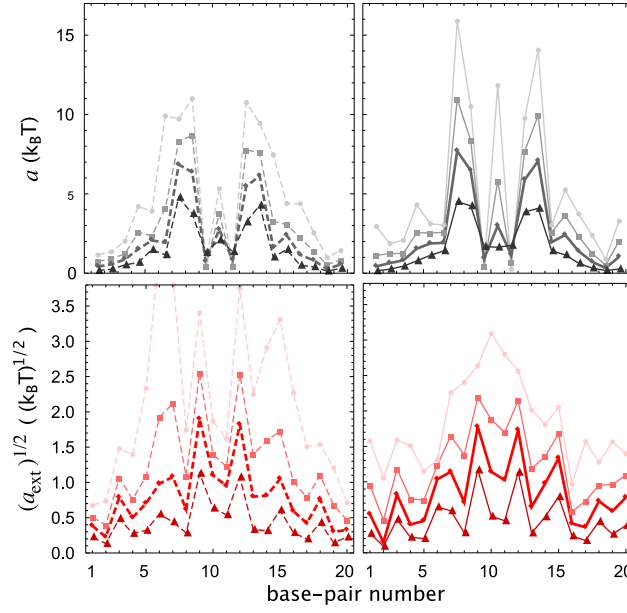


Figure *supp-2*: The magnitude of base-pair forces and torques resulting from nano-mechanics analysis depends on the range of allowed pre-relaxation  $r_m$ . Generally, wider allowed relaxation ranges result in a reduction of global force and energy scale, scaling roughly as  $r_m^{-1}$ . In addition, for the smaller values of  $r_m$  the profile shapes also change. The first row of the figure shows energy profiles for *Ippo-I*. The curves correspond to: no relaxation and  $r_m = 0.15, 0.3, 0.6\text{\AA}$ , from top to bottom in each panel. The value  $r_m = 0.3\text{\AA}$  equals to the reported atomic position uncertainty, used in Fig. 6. MP parameter set, left column; P parameter set, right column. The second row shows the combined magnitude of external force and torque, computed from the energy  $a_{\text{ext}}(\mu(k))$  associated with a force-torque pair:  $a_{\text{ext}}(\mu(k)) = \frac{1}{2}\mu(k)^\top (\mathbf{S}_{(b_{k-1}b_k)} + \mathbf{A}_{kk+1}^\top \mathbf{S}_{(b_k b_{k+1})} \mathbf{A}_{kk+1})^{-1} \mu(k)$ . Values of  $r_m$  and parameter sets as above.